Supporting information

Luminescent Phosphine Copper(I) Complexes with Various Functionalized Bipyridine Ligands: Synthesis, Structures, Photophysics and Computational Study

Xin-Xin Jin, [a,+] Tian Li, [b,+] Dong-Po Shi, [a,+] Li-Juan Luo,[a] Qian-Qian Su,[a,] Jing Xiang,[a,*] Hai-Bing Xu,[b] Chi-Fai Leung, [c,*] Ming-Hua Zeng [b*]

[a] *College of Chemistry and Environmental Engineering, Yangtze University, Jingzhou 434020, Hubei, P. R. China. Email: xiangjing@yangtzeu.edu.cn*

[b] *Hubei Collaborative Innovation Center for Advanced Organic Chemical Materials, Ministry-of-Education Key Laboratory for the Synthesis and Application of Organic Functional Molecules & College of Chemistry & Chemical Engineering, Hubei University, Wuhan 430062 (China)*

c Department of Science and Environmental Studies, The Education University of Hong Kong, 10 Lo Ping Road, Tai Po, Hong Kong, China

[+] these authors contributed equally

Table of supporting information

Experimental section

Physical Measurements and Instrumentation. ^{1}H NMR and $^{31}P\{^{1}H\}$ NMR spectra were recorded on a Bruker AV300 (300 MHz) FT-NMR spectrometer. Chemical shifts (δ, ppm) are reported relative to tetramethylsilane (Me_4Si). Elemental analysis was performed on an Elementar Vario MICRO Cube elemental analyzer. IR spectra of the solid samples as KBr discs were obtained within the range 4000–400 cm^{-1} on an AVATAR 360 FTIR spectrometer. All of the electronic absorption spectra were recorded on a Hewlett–Packard 8453 or Hewlett–Packard 8452A diode-array spectrophotometer. Steady-state emission spectra were measured at room temperature and at 77 K on a Horiba Jobin Yvon Fluorolog-3-TCSPC spectrofluorometer. The solutions were rigorously degassed on a high-vacuum line in a two-compartment cell with not less than four successive freeze–pump–thaw cycles. The measurements at 77 K were carried out on dilute solutions of the samples in EtOH/MeOH (4:1, v/v) loaded in a quartz tube inside a quartz-walled Dewar flask that contained liquid nitrogen. Luminescence lifetimes were measured by using the time-correlated single-photon-counting (TCSPC) technique on a Fluorolog-3-TCSPC spectrofluorometer in a fast MCS mode with a Nano LED-375 LH excitation source, which had a peak excitation wavelength at 375 nm and a pulse width of less than 750 ps. The photon-counting data were analyzed on Horiba Jobin Yvon Decay Analysis Software.

X-ray Crystallography. The crystal structures were determined on an Oxford Diffraction Gemini S Ultra X-ray single-crystal diffractometer using graphite-monochromated Cu K_a radiation (λ = 1.5417 Å). The structures were solved by using direct methods with the SHELXS-97 program[1]. The Cu metal atom and many of the non-hydrogen atoms were located according to the direct methods. The positions of the other non-hydrogen atoms were located after refinement by full matrix least-squares by using the SHELXL-97 program.[2] In the final stage of the least-squares refinement, all non-hydrogen atoms were refined anisotropically. H atoms were generated by SHELXL-97 program. The positions of H atoms were calculated based on riding model with thermal parameters that were 1.2 times that of the associated C atoms and participated in the calculation of the final Indices. Structures reported in this paper have been deposited to the Cambridge Crystallographic Data Centre (CCDC) with the depository numbers CCDC 1943787-1943789.

Computational Details. All the calculations were done by GAUSSIAN 09, version B.01.[3] The ground state and lowest triplet state structures of complexes **1**, **4**, **5** were optimized using B3LYP functional[4] and a mixed basis set of 6-31+G(d) (for C, H, N, P) and LANL2DZ[5] (for Cu). To reduce computation complexity, the phenyl rings of $P(PhX)_3$ or POP ligands are replaced by methyl groups. Polarized Continuum Model[6] (PCM) was employed to account for the solvent effect. Frequency calculations were done after optimization and no imaginary frequencies were found. The X-ray crystal structures of the complexes were used without further optimization.

Reference:

(1) G. M. Sheldrick, SHELX-97: Programs for Crystal Structure Analysis, release 97-2, University of Gottingen, Germany, 1997.

(2) A. Altomare, G. Cascarano, C. Giacovazzo, A. Guagliardi, M. Burla, G. Polidori and M. Camalli, *J. Appl. Crystallogr*., 1994, **27**, 435.

(3) M. J. Frisch, G. W. Trucks, H. B. Schlegel et al., *Gaussian 09*, Revision B.01, Gaussian, Inc., Wallingford CT, 2009

(4) (a) A. D. Becke, *J. Chem. Phys.* 1993, **98**, 5648-5652; (b) C. Lee, W, Yang, R. G. Parr, *Phys. Rev. B*, 1988, **37**, 785; (c) P. J. Stephens, F. J. Devlin, C. F. Chabalowski, M. J. Frisch, *J. Phys. Chem.* 1994, **98**, 11623-11627.

(5) (a) Y. Zhao and D. G. Truhlar, *Theor. Chem. Acc.*, 2008, **120**, 215–241; (b) A. Schäfer, H. Horn and R. Ahlrichs, *J. Chem. Phys.* 1992, **97**, 2571–2577; (c) W. R. Wadt and P. J. Hay, *J. Chem. Phys.* 1985, **82**, 284–298.

(6) G. Scalmani and M. J. Frisch, *J. Chem. Phys.* 2010, **132**, 114110.

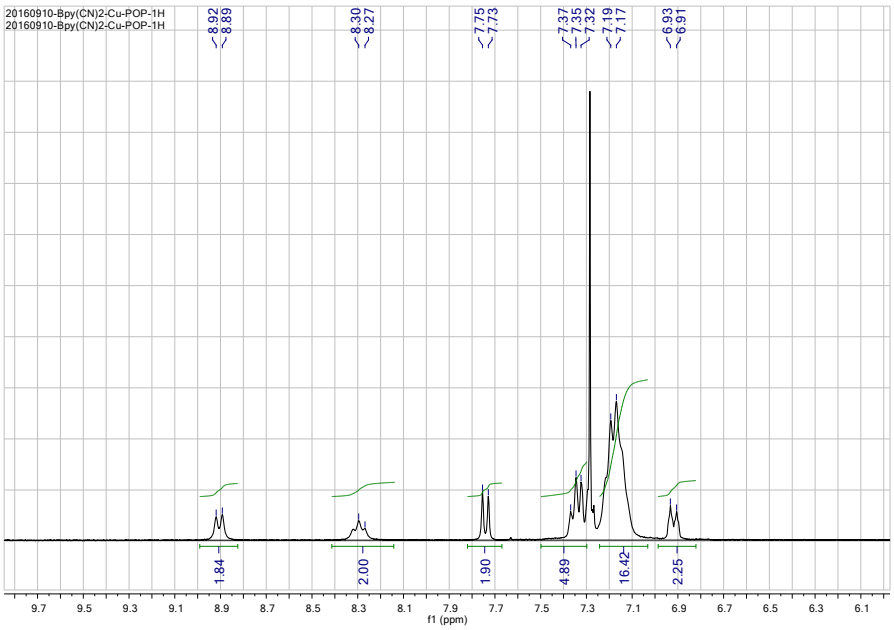

Figure S1. ^{1}H NMR spectroscopy of **4**.

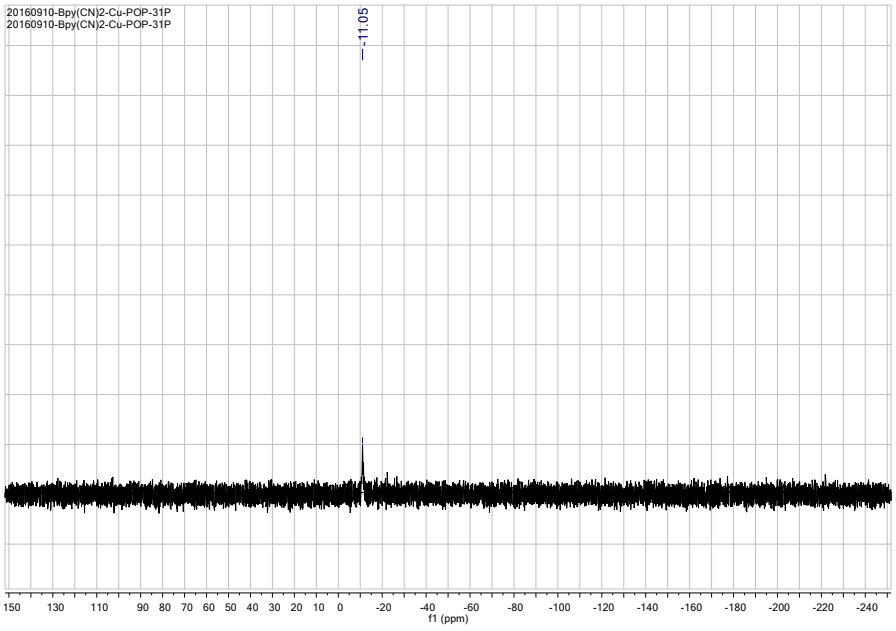

Figure S2. ^{31}P{1H} NMR spectroscopy of **4**.

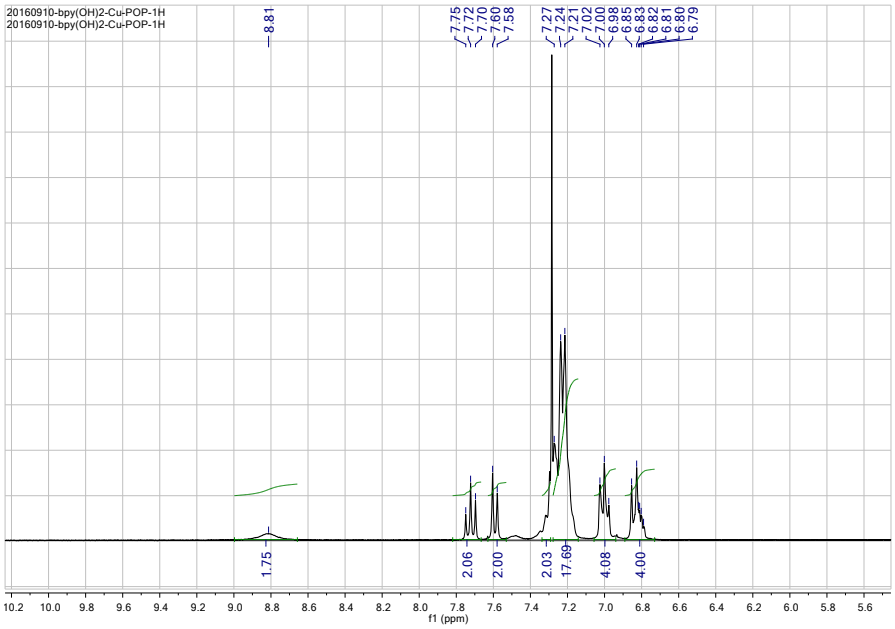

Figure S3. ^{1}H NMR spectroscopy of **6**.

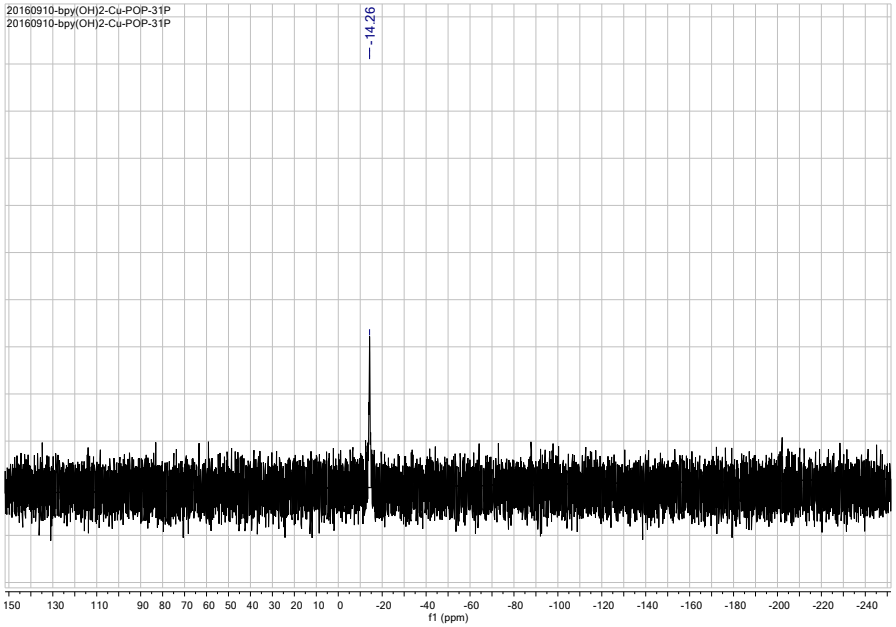

Figure S4. ^{31}P{1H} NMR spectroscopy of **6**.

Table S1. Crystal data and structure refinement details for compounds **1**, **4**, **5**.

	1	**4**	**5**
Formula	$C_{48}H_{36}ClCuN_4O_4P_2$	$C_{48}H_{34}ClCuN_4O_5P_2$	$C_{48}H_{44}ClCuN_2O_7P_2$
Mr	893.74	907.72	921.78
T /K	293 (2) K	293 (2) K	293 (2) K
Crystal syst	Monoclinic	Monoclinic	Triclinic
Space group	$P2_1/c$	$C2/c$	*P-1*
a/Å	10.9189 (10)	25.2095 (6)	11.0935 (9)
b/Å	31.935 (2)	11.1731 (3)	12.6712 (12)
c/Å	12.9477 (15)	31.1132 (7)	16.9260 (12)
α, (°)	90	90	90.048 (7)
β, (°)	103.968 (10)	90.061 (2)	101.514 (6)
γ, (°)	90	90	100.446
V/ Å^3	4381.3 (7)	8763.6 (4)	2291.0 (3)
Z	4	8	2
ρ_{calcd}, Mg m^{-3}	1.355	1.376	1.336
F(000)	1840	3728	956
Collected refl.	14886	27379	14695
Unique refl.	7839	7864	8204
R(int)	0.075	0.044	0.068
Final *R* indices, *I* > 2σ(I)	R_1(obs)=0.083 *w*R(all)=0.262	R_1(obs)=0.086 *w*R(all)=0.279	R_1(obs)= 0.069 *w*R(all)= 0.184
GOF	1.05	1.03	0.99
No.of par.	560	587	552

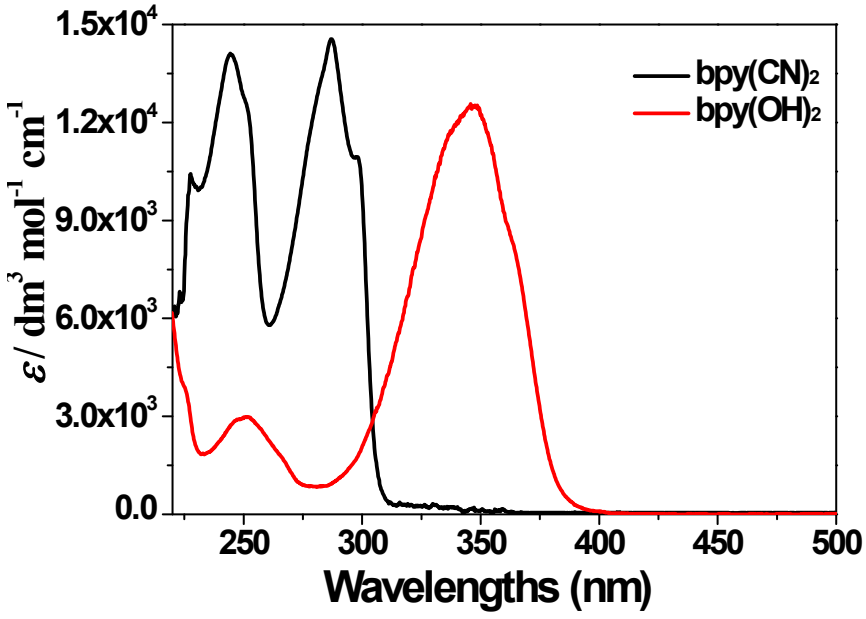

Figure S5. The UV-Vis spectra of ligands **bpy(CN)$_2$** and **bpy(OH)$_2$**.

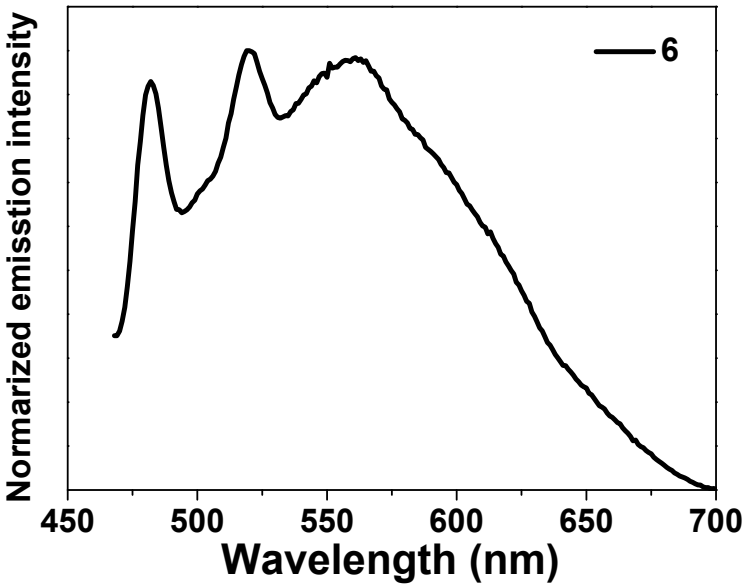

Figure S6. The emission spectra of **6** in EtOH-MeOH (4:1, v/v) glassy medium at 77 K (λ_{ex} = 355 nm).

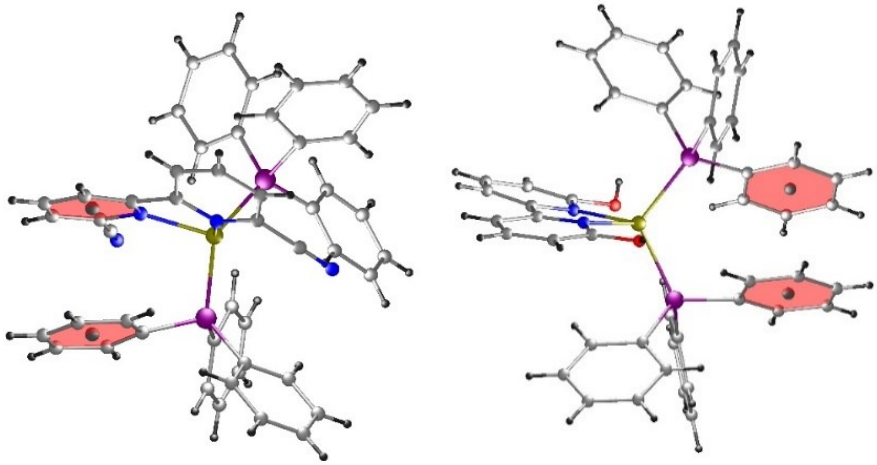

Figure S7. The intra-molecular π-π stacking found in **1** (left) and **5** (right).

Table S2 Calculated transition energies and the changes in the electron densities of the lowest 10 vertical transitions of **1**

λcalc / nm (Oscillator Strength)	**Changes of the electron density (% contribution; H: HOMO, L: LUMO)**	**Transition Characters**
453.45 nm (0.0392)	H→L (96.7%)	MLCT[d(Cu) →π*(**L1**)]

435.38 nm (0.0096)	H-2→L (2.0%), H-1→L (94.6%)	MLCT[d(Cu)→π*(**L**[1])]
385.01 nm (0.0074)	H-1→L+1 (20.8%), H→L+2 (77.2%)	MLCT[d(Cu)→π*(**L**[1])]
313.95 nm (0.0087)	H-4→L (14.4%), H-3→L (5.0%), H-9→L (66.3%), H-7→L (11.0%)	MLCT[d(Cu)→π*(**L**[1])]
308.77 nm (0.0068)	H-14→L (67.3%), H-13→L (3.1%), H-9→L (14.8%), H-7→L (2.2%), H-5→L+1 (2.8%), H-3→L +1(2.5%)	MLCT[d(Cu)→π*(**L**[1])]
306.69 nm (0.0176)	H-16→L (13.0%), H-15→L (5.6%), H-10→L (71.6%), H-4→L (3.5%)	MLCT[d(Cu)→π*(**L**[1])]
297.81 nm （0.0211）	H-17→L+1 (2.7%), H-12→L (2.3%), H-12→L+1 (3.9%), H-11→L+1 (26.9%), H-10→L (2.1%), H-10→L +1(3.9%)	MLCT[d(Cu)→π*(**L**[1])]
295.61 nm (0.0317)	H-15→L+1 (23.1%), H-10→L+1 (5.7%), H-8→L+1 (9.1%), H-5→L+2 (11.7%)	MLCT[d(Cu)→π*(**L**[1])]
292.53 nm (0.0505)	H-17→L (20.5%), H-17→L+1 (2.3%), H-16→L (3.6%), H-16→L+1 (3.1%), H-12→L+1 (18.1%), H-10→L+1 (21.4%), H-8→L+1 (2.0%), H-5→L+2 (12.8%), H-4→L+1 (4.9%)	MLCT[d(Cu)→π*(**L**[1])]
286.92 nm (0.0159)	H-17→L (2.2%), H-17→L+1 (5.0%), H-16→L+1 (11.2%), H-15→L+1 (11.5%), H-12→L+1 (18.5%), H-11→L+1 (3.4%), H-10→L+1 (9.6%), H-8→L+1 (5.9%), H-7→L+2 (9.1%), H-5→L+2 (19.5%)	MLCT[d(Cu)→π*(**L**[1])]

Table S3 Calculated transition energies and the changes in the electron densities of the lowest 10 vertical transitions of **4.**

λ_{calc} / nm (Oscillator Strength)	**Changes of the electron density (% contribution; H:HOMO, L:LUMO)**	**Transition Characters**

444.37 nm (0.0049)	H→L (94.8%)	MLCT[d(Cu) →π*(**L**^{1})]
410.97 nm (0.0124)	H-2→L+2 (2.0%), H-2→L+3 (94.5%)	MLCT[d(Cu)→π*(**L**^{1})]
404.47 nm (0.0108)	H-11→L (2.7%), H-8→L+1 (4.3%), H-7→L (5.0%), H-6→L (47.6%), H-5→L (6.1%), H→L+5 (3.2%), H→L+7 (19.1%),	MLCT[d(Cu)→π*(**L**^{1})]
401.47 nm (0.1066)	H-5→L (3.4%), H-1→L+4 (84.5%)	MLCT[d(Cu)→π*(**L**^{1})]
383.37 nm (0.0117)	H-11→L (9.4%), H-10→L (6.3%), H-8→L (50.3%), H-7→L (3.3%), H-6→L (7.8%), H-5→L (6.4%), H-1→L+4 (4.5%),, H→L+8 (2.1%)	MLCT[d(Cu)→π*(**L**^{1})]
367.58 nm (0.0158)	H-10→L (2.2%), H-7→L (3.2%), H→L +8(47.0%), H→L+10 (28.3%), H→L+12 (3.0%), H→L+13 (5.3%)	MLCT[d(Cu)→π*(**L**^{1})]
355.11 nm (0.0123)	H-14→L (2.7%), H-13→L (4.4%), H-1→L+5 (17.5%), H-1→L+7 (5.9%), H→L+8 (4.2%), H→L+10 (5.6%), H→L+11 (8.8%), H→L+12 (4.5%), H→L+13 (33.1%)	MLCT[d(Cu)→π*(**L**^{1})]
349.34 nm (0.0189)	H-16→L (5.8%), H-15→L (5.6%), H-12→L (30.0%), H-11→L (5.5%), H-10→L (13.3%), H-8→L (5.2%), H-1→L+5 (5.0%), H-1→L +6(3.0%), H-1→L+7 (8.0%), H→L+13 (7.5%)	MLCT[d(Cu)→π*(**L**^{1})]
348.05 nm (0.0150)	H-16→L (15.6%), H-12→L (7.0%), H-10→L (8.0%), H-1→L+5 (21.7%), H-1→L+7 (9.4%), H→L+12 (2.5%), H→L+13 (21.1%)	MLCT[d(Cu)→π*(**L**^{1})]
347.04 nm (0.0295)	H-12→L (2.3%), H-1→L+5 (5.6%), H-1→L+6 (59.6%), H-1→L+7 (14.3%), H→L+13 (3.0%)	MLCT[d(Cu)→π*(**L**^{1})]

Table S4 Calculated transition energies and the changes in the electron densities of the lowest 10 vertical transitions of **5.**

λ_{calc} / nm (Oscillator Strength)	Changes of the electron density (% contribution; H:HOMO, L:LUMO)	Transition Characters
437.30 nm (0.0022)	H-2→L+1 (12.2%), H-1→L+1 (36.2%), H→L (42.9%), H-7→L+1 (6.5%),	MLCT[d(Cu)→ π*(PPh_3)] + LLCT[π(**L^2**)→π*(PPh_3)]
432.96 nm (0.0043)	H-2→L+1 (7.1%), H-1→L+1 (59.6%), H-9→L+1(31.2%)	LLCT[π (PPh_3) →π*(**L^2**)] + MLCT[d(Cu)→ π*(PPh_3)]
429.02 nm (0.0323)	H-8→L (4.6%), H-7→L (65.4%), H-10→L +1(7.2%), H-2→L+2 (16.3%)	MLCT[d(Cu)→ π*(PPh_3)] + LLCT[π(PPh_3) →π*(**L^2**)]
428.88 nm (0.0196)	H-18→L+1 (2.2%), H-14→L+1 (3.3%), H-5→L +2(3.1%), H-3→L+2 (84.1%)	LLCT[π(PPh_3) →π*(**L^2**)] + MLCT[d(Cu)→ π*(PPh_3)]
421.72 nm (0.0019)	H-12→L+1 (77.7%), H-9→L+1 (21.1%)	LLCT[π(PPh_3) →π*(**L^2**)] + MLCT[d(Cu)→ π*(PPh_3)]
415.91 nm (0.0026)	H-18→L (2.2%), H-13→L+1 (79.2%), H-10→L+1(13.9%)	LLCT[π(PPh_3) →π*(**L^2**)] + MLCT[d(Cu)→ π*(PPh_3)]
413.80 nm (0.0168)	H-18→L (53.4%), H-13→L+1 (5.3%), H-4→L+2(14.7%), H-2→L+2 (22.4%),	LLCT[π(PPh_3) →π*(**L^2**)] + MLCT[d(Cu)→ π*(PPh_3)]
410.53 nm (0.0018)	H-19→L (6.9%), H-18→L+1 (3.4%), H-14→L+1(80.2%), H-3→L+2 (4.8%),	LLCT[π(PPh_3) →π*(**L^2**)] + MLCT[d(Cu)→ π*(PPh_3)]
404.51 nm (0.0251)	H-19→L (89.2%), H-14→L+1 (6.2%)	MLCT[d(Cu)→ π*(PPh_3)] + LLCT[π(PPh_3) →π*(**L^2**)]
399.13 nm (0.0108)	H-16→L+1 (2.3%), H-15→L+1 (95.5%)	MLCT[d(Cu)→ π*(PPh_3)] + LLCT[π(PPh_3) →π*(**L^2**)]